

# Quantum Well Infrared Photodetectors: Device Physics and Light Coupling

S. V. Bandara, S. D. Gunapala, J. K. Liu, J. Mumolo, E. Luong, W. Hong and D. K. Sengupta

Center for Space Microelectronics Technology

Jet Propulsion Laboratory

California Institute of Technology

Pasadena, CA 91109

## Introduction

It is customary to make infrared (IR) detectors in the long wavelength range (8 -20  $\mu\text{m}$ ) by utilizing the interband transition which promotes an electron across the band gap ( $E_g$ ) from the valence band to the conduction. These photo-electrons can be collected efficiently, thereby producing a photocurrent in the external circuit. Since the incoming photon has to promote an electron from the valence band to the conduction band, the energy of the photon ( $h\nu$ ) must be higher than the  $E_g$  of the photosensitive material. Therefore, the spectral response of the detectors can be controlled by controlling the  $E_g$  of the photosensitive material and detection of very long wavelength IR radiation up to 20  $\mu\text{m}$  requires small band gaps down to 62 meV. Examples of such materials meeting these requirements are  $\text{Hg}_{1-x}\text{Cd}_x\text{Te}$  and  $\text{Pb}_{1-x}\text{Sn}_x\text{Te}$  in which the energy gap can be controlled by varying  $x$ . It is well known that these low band gap materials are more difficult to grow and process than large band gap semiconductors such as GaAs. These difficulties motivate the exploration of utilizing the intersubband transitions in multi quantum well (MQW) structures made of large band gap semiconductors .

The detection mechanism of Quantum Well Infrared Photodetector (QWIP) involves photoexcitation of electrons between ground and first excited states of single or a multi-quantum well structure. The parameters are designed so that these photo excited carriers can escape from the well and be collected as photocurrent.<sup>1,2</sup> These quantum wells can be realized by placing thin layers of two different high bandgap semiconductor materials alternately where the bandgap discontinuity creates potential wells associated with conduction bands and valence bands. Currently, there is a great interest in the GaAs/ $\text{Al}_x\text{Ga}_{1-x}\text{As}$  based QWIP because modern crystal-growth methods like molecular beam epitaxy (MBE) allow the growth of highly uniform

and pure crystal layers of such semiconductors on large substrate wafers, with control of each layer thickness down to a fraction of a molecular layer. The GaAs/Al<sub>x</sub>Ga<sub>1-x</sub>As material system allows the quantum well shape to be tweaked over a range wide enough to enable light detection at any narrow wavelength range within 6-20 μm.<sup>1-3</sup>

## Dark Current

Improving QWIP performance depends largely on minimizing the dark current that flows through a biased detector with no photons impinging on it. In QWIPs, the dark current originates from three different mechanisms.<sup>4-6</sup> As shown in Fig. 1, the dark current arising from the first process is due to quantum mechanical tunneling from well to well through the Al<sub>x</sub>Ga<sub>1-x</sub>As barriers (sequential tunneling). This process is independent of temperature. Sequential tunneling dominates the dark current at very low temperatures (<30 K). The second mechanism is thermally assisted tunneling which involves a thermal excitation and tunneling through the tip of the barrier into the continuum energy levels. This process governs the dark current at medium temperatures. The third mechanism is classical thermionic emission and it dominates the dark current at higher temperatures (>55 K for 9 μm cutoff QWIPs). The thermal generation rate associated with this current depends on the well doping density and the life time of the carriers which will be determined by the thickness of the Al<sub>x</sub>Ga<sub>1-x</sub>As barriers. Consequently, for QWIPs operating at higher temperatures the last mechanism is the major source of dark current<sup>4,6</sup>

In order to optimize the performance of the QWIP, a *bound-to-quasibound* quantum well was developed by placing the first excited state exactly at the well top as shown in Fig. 2. Dropping the first excited state to the well top causes the barrier to thermionic emission (roughly the energy height from the ground state to the well top) to be - 10-15 meV more than that of the bound-to-continuum (the first excited state lies in the continuum energy band above the well top) QWIP.<sup>4</sup> The dark current-voltage curve of the 15 μm peaked bound-to-quasibound QWIP is shown in Fig. 2. This compares well with the experimentally observed more than 10 factor drop compare to the *bound-to-continuum* QWIP having the same peak wavelength.

## Spectral Response

Unlike the responsivity spectrums of intrinsic infrared detectors, the responsivity spectrums of QWIPs are much narrower and sharper due to their resonance intersubband absorption.<sup>1,2</sup> The normalized responsivity spectra  $R(\lambda)$  are given in Fig. 3, where we see that the *bound* and *quasibound* excited state QWIPs are much narrower  $\Delta\lambda/\lambda - 10\%$  than the *continuum* QWIPs  $\Delta\lambda/\lambda = 24\%$ . This is due to the fact that when the excited state placed in the continuum band above the barrier the energy width associated with the state becomes wider. Spectral band width becomes wider. Spectral band width of these QWIPs can be further increased by increasing the carrier density and by slightly varying the parameters of the quantum wells of the multi-quantum well structure.<sup>7</sup> See Figure 4. This device structure involved several repeated layers of three different GaAs/ $\text{Al}_x\text{Ga}_{1-x}\text{As}$  quantum wells separated thick  $\text{Al}_x\text{Ga}_{1-x}\text{As}$  barriers. The thickness of the GaAs layer of these three quantum wells are designed to respond at peak wavelengths 13.5  $\mu\text{m}$ , 14.3  $\mu\text{m}$  and 15.5  $\mu\text{m}$  respectively. These measurements show broadening of the spectral response up to  $\Delta\lambda - 6\ \mu\text{m}$ , i.e. the full width at the half maximum from 13.2 -16.6  $\mu\text{m}$ . This broadening  $\Delta\lambda/\lambda_p - 46\%$  is more than 400 % increase comparing to a typical bound-to-quasibound QWIP. This band width can be tuned to a desired value by varying the structure parameters.<sup>7</sup>

The absolute peak responsivity  $R_p$  can be written in terms of quantum efficiency  $\eta$  and photoconductive gain  $g$  as  $R_p = (e/h\nu)\eta g$ . The bias dependence of  $R_p$  is shown in Fig. 5. Note that at low bias the responsivity is nearly linearly dependent on bias and it saturates at high bias. This saturation occurs due to the saturation of carrier drift velocity. The responsivity of more *bound-to-bound* samples has a significantly different shape. The responsivity does not start out linearly with bias but is in fact zero for finite bias. That is, there is a zero bias offset of more than 1 V, due to the necessity of field assisted tunneling for the photoexcited carrier to escape from the well.

At low operating bias voltages, responsivity spectrum of bound-to-bound QWIPs show additional peaks due to resonance energy levels of potential barriers. See Figure 6. Although the absorption between ground state and barrier resonance levels are much smaller than that of the ground and first excited state, at lower bias voltages escape probability of the photoexcited

electrons at the bounded first excited state is much smaller. When the bias the escape probability of the photoexcited electrons at the excited state (bounded to the well) also increases. Thus the peak associates with the bound to excited transition becomes dominant in the spectrum. Also, due to the same reason, bound-to-continuum QWIPs do not show any responsivity peaks associated with barrier resonances.

## Light Coupling

QWIPs do not absorb radiation incident normal to the surface since the light polarization must have an electric field component normal to the superlattice (growth direction) to be absorbed by the confined carriers<sup>1,2</sup>. When the incoming light contains no polarization component along the growth direction, the matrix element of the interaction vanishes (i.e.,  $\vec{\epsilon} \cdot \vec{p}_z = 0$  where  $\vec{\epsilon}$  is the polarization and  $\vec{p}_z$  is the momentum along z direction). As a consequence, these detectors have to be illuminated through a 45° polished facet<sup>1,2</sup>. Clearly, this illumination scheme limits the configuration of detectors to linear arrays and single elements. For imaging, it is necessary to be able to couple light uniformly to two dimensional arrays of these detectors.

Several different monolithic grating structures, such as linear gratings<sup>8,9</sup>, two-dimensional (2-D) periodic gratings<sup>10-12</sup>, and random-reflectors<sup>13,14</sup> have been demonstrated for efficient light coupling to QWIPs, and has made two dimensional QWIP imaging arrays' feasible. These gratings deflect the incoming light away from the direction normal to the surface, enabling intersubband absorption. These gratings were made of metal on top of each detector or crystallographically etched through a cap layer on top of the MQW structure. Normal incident light-coupling efficiency comparable to the light coupling efficiency of a 45° polished facet illumination was demonstrated using linear gratings<sup>8,9</sup>.

Detailed theoretical analysis<sup>11</sup> has been carried out on both linear and 2-D periodic gratings for QWIPs. In 2-D gratings, the periodicity of the grating repeats in two perpendicular directions on the detector plane, leading to the absorption of both polarizations of incident IR radiation. Also, experiments have been carried out for two-dimensional grating coupled QWIP detectors designed for wavelengths  $\lambda - 9 \mu\text{m}$ <sup>10</sup> and  $\lambda - 16 - 17 \mu\text{m}$ <sup>14</sup>. A factor of 2-3

responsivity enhancement relative to the standard  $45^\circ$  polished facet illumination was observed for large area mesas (  $500 \text{ nm} \times 500 \text{ }\mu\text{m}$  ) with total internal reflection optical cavity which can be created with an additional AlGaAs layer<sup>10,11</sup> or with a thinned substrate<sup>12</sup>. This optical cavity is responsible for about an extra enhancement factor of two due to the total internal reflection from the AlGaAs layer or from the thinned substrate (Fig. 7).

Random reflectors have demonstrated excellent optical coupling for individual QWIPs as well as for large area focal plane arrays<sup>13,14</sup>. It has been shown that many more passes of IR light (Fig. 7), and significantly higher absorption, can be achieved with a randomly roughened reflecting surface. By careful design of surface texture randomization (with three level random reflector), an enhancement factor-of-eight in responsivity compared to  $45^\circ$  illumination was demonstrated experimentally<sup>13</sup>. The random structure on top of the detector prevents the light from being diffracted normally backward after the second bounce as happens in the case of 2-D periodic grating. See Fig. 7. Naturally, thinning down the substrate enables more bounces of light and therefore higher responsivity<sup>13</sup>.

All these gratings were fabricated on the detectors by using standard photolithography and selective dry etching. The advantage of the photolithographic process is its ability to accurately control the feature size and to preserve the pixel-to-pixel uniformity, which is a prerequisite for high-sensitivity imaging focal plane array. However the resolution of the photolithography and the accuracy of etching processes become key issues in producing smaller grating feature sizes. These feature sizes are proportionally scaled with the peak response wavelength of the QWIP. It is important to note that for any given wavelength the random grating requires much smaller feature sizes than two dimensional periodic gratings.<sup>15</sup> The minimum feature size of the random reflectors of  $15 \text{ }\mu\text{m}$  and  $9 \text{ }\mu\text{m}$  cutoff FPAs were  $1.25 \text{ }\mu\text{m}$  and  $0.6 \text{ }\mu\text{m}$  respectively.<sup>15</sup> Thus, the random reflectors of the  $9 \text{ }\mu\text{m}$  cutoff FPA were less sharp and had fewer scattering centers compared to random reflectors of the  $15 \text{ }\mu\text{m}$  cutoff FPA and this is due to the difficulties associated with sub-micron photolithography. These less sharp features in random gratings lowered the light coupling efficiency than expected. Thus, it could be advantageous to utilize a 2-D periodic grating for light coupling in shorter wavelength QWIPs.

The normalized responsivity spectrum for 2-D periodic grating coupled QWIP samples (with six different grating periods,  $D$  and a fixed groove depth,  $h$ ) and for the standard  $45^\circ$  sample are shown in Fig. 8. Note the normalized spectral peak shifts from  $7.5 \mu\text{m}$  to  $8.8 \mu\text{m}$  as the grating period increases from  $D = 2.2 \mu\text{m}$  to  $3.2 \mu\text{m}$ . These measurements were repeated for three groove depths. The grating peak wavelength  $\lambda_{gp}$  (where the grating enhancement is maximized) and the peak enhancement (enhancement at  $\lambda_{gp}$ ) associated with each grating period was obtained by normalizing the absolute spectral responsivity of the grating detectors relative to the  $45^\circ$  detector sample. Fig. 9 shows the variation of the grating peak wavelength with grating period for samples with three different groove depths. As expected from the theory,  $\lambda_{gp}$  linearly depends on the grating period and it is independent of the groove depth of the grating.

Fig. 10 shows the experimental data and theoretical comparison for responsivity enhancement due to 2-D periodic gratings. Theoretical curves were plotted as a function of groove depth ( $h$ ) for different feature sizes ( $d$ ) normalized to characteristic grating peak wavelength in GaAs,  $\lambda_{gp}(\text{GaAs})$ . Feature sizes  $d$  for each grating were obtained using SEM pictures of each grating. Although the normalized feature size  $d/\lambda_{gp}(\text{GaAs})$  is the same for all the gratings, SEM measurements show slight variations. These variations can be attributed to the limitations of device fabrication processes such as photolithography and metal ization.

## SUMMARY

In summary, QWIPs afford greater flexibility than the usual extrinsically doped semiconductor IR detectors because the wavelength of the peak response and cutoff can be continuously tailored by varying layer thickness (well width), barrier composition (barrier height), and carrier density (well doping density). The GaAs/ $\text{Al}_x\text{Ga}_{1-x}\text{As}$  material system allows the quantum well parameters to be varied over a range wide enough to enable light detection at any wavelength range between 6-20  $\mu\text{m}$ . The spectral band width of these detectors can be tuned from narrow ( $\Delta\lambda/\lambda - 10\%$ ) to wide ( $\Delta\lambda/\lambda - 40\%$ ) allowing various applications. Also, we have observed an enhancement factor of three due to 2D periodic grating fabricated on QWIP

structure. Variation of the enhancement factor with groove depth and feature size of the grating can be theoretically explained. However the resolution of the photolithography and accuracy of the etching become key issues in producing smaller grating feature sizes especially in shorter wavelengths. Unlike random reflectors the light coupling efficiency of two dimensional (2-D) gratings strongly depends on the wavelength and thus exhibits narrow band width spectral responses.

## ACKNOWLEDGMENTS

The research described in this paper was performed by the Center for Space Microelectronics Technology, Jet Propulsion Laboratory, California Institute of Technology, and was sponsored by the National Aeronautics and Space Administration, Office of Space Science,

## References

1. S. D. Gunapala and K. M. S. V. Bandara, in *Physics of Thin Films*, edited by M. H. Francombe and J. L. Vossen, Vol. 21, pp. 113-237, Academic Press, NY, 1995.
2. B. F. Levine, *J. Appl. Phys.* 74, R1 (1993).
2. K. K. Choi, *J. Appl. Phys.* 73, 5230 (1993).
4. B. F. Levine, C. G. Bethea, G. Hasnain, V. O. Shen, E. Pelve, R. R. Abbott, and S. J. Hsieh, *Appl. Phys. Lett.*, 56, 851 (1990).
5. E. Pelve, F. Beltram, C. G. Bethea, B. F. Levine, V. O. Shen, S. J. Hsieh, R. R. Abbott, *J. Appl. Phys.* 66, 5656 (1989).
6. S. D. Gunapala, J. K. Liu, J. S. Park, M. Sundaram, C. A. Shott, T. Helter, T. L. Lin, S. T. Massie, P. D. Maker, R. E. Muller, and G. Sarusi, *IEEE Trans. Ele. Devices*, vol. 44, 45-59 (1997).
7. S. V. Bandara, S. D. Gunapala, J. K. Liu, J. Mumolo, E. Luong, W. Hong and D. K. Sengupta, to be published.
8. K. W. Goossen, S. A. Lyon, *J. Appl. Phys.*, vol. 63, 5149 (1988).

9. G.Hansain, B. F. Levine, C'. G.Bethea,R. A. Logan, J. Walker, and R.J. Malik, *Appl. Phys.lett.*,vol. 54,2515 (1989).
10. J. Y. Andersson and L. Lundqvist, *Appl. Phys, Lett.* vol. 59, 857(1 991).
11. J. Y. Andersson, L. Lundqvist and Z.F. Paska, *J. Appl. Phys.* vol. 71,3600 (1991).
12. G.Sarusi, B. F. Levine, S. J. Pearton, K. M. S. V. Bandara, R. E. Leibenguth, and J. Y. Andersson *J. Appl. Phys.*, vol. 76, 4989(1994).
13. B. Xing, and H. C, Liu, *J. Appl. Phys.*, vol. 80, 1214 (1996).
14. G. Sarusi, B. F. Levine, S. J. Pearton, K. M. S. V. Bandara, and R. E. Leibenguth, *Appl. Phys. Lett.*, vol. 64, pp. 960-962,(1994).
15. S. Bandara, S. Gunapala, J. Liu, W. Hong and J. Park, *SPIE Vol.* 2999, 103 (1 997).

## Figure Captions

Fig. 1 Schematic diagram of the conduction band in a bound-to-quasibound QWIP in an externally applied electric field. Absorption of IR photons can photoexcite electrons from the ground state of the quantum well into the continuum, causing a photocurrent. Three dark current mechanisms are also shown: ground state tunneling (1); thermally assisted tunneling (2); and thermionic emission (3). The inset shows a cross-section transmission electron micrograph of a QWIP sample.

Fig. 2 Comparison of dark currents of bound-to-continuum and bound-to-quasibound QWIPs as a function of bias voltage at temperature  $T = 55$  K.

Fig. 3 Spectral band width variation of QWIPs with bound-to-bound, bound-to-quasibound and bound-to-continuum transitions.

Fig. 4 Normalized spectral responsivity of broad-band QWIPs.

Fig.5. Bias dependent peak ( $\lambda = \lambda_p$ ) responsivity of QWIPs with bound-to-bound, bound-to-quasibound and bound-to-continuum transitions.

Fig.6. Normalized spectral responsivity of a bound-to-bound QWIPs showing additional peak due to barrier resonance at lower bias voltages.

Fig. 7 (a) Schematic side view of a thin QWIP pixel with a random grating reflector. Ideally all the radiation is trapped except for a small fraction which escapes through the escape cone. (b) Schematic diagram of 2-D periodic grating specifications. The grating features are spaced periodically along the x and y directions.

Fig. 8 Measured normalized responsivity spectra as a function of grating, period  $D$  for  $D=2.2 - 3.2$   $\mu\text{m}$ . The bold curve represent responsivity spectra same QWIP with  $45^\circ$  polished edge.

Fig. 9. Measured grating peak wavelength  $\lambda_{gp}$  vs the grating period for samples with three different groove depths  $h$ .

Fig.10 The experimental data (solid circles) and theoretical comparison of responsivity enhancement in 2-D periodic grating coupled QWIP. Theoretical curves were plotted as a function of groove depth,  $h$  for different feature sizes  $d$  normalized to characteristic grating peak wavelength in GaAs,  $\lambda'_{gp}$ . Feature sizes  $d$  for each grating were obtained using SEM pictures of each grating.

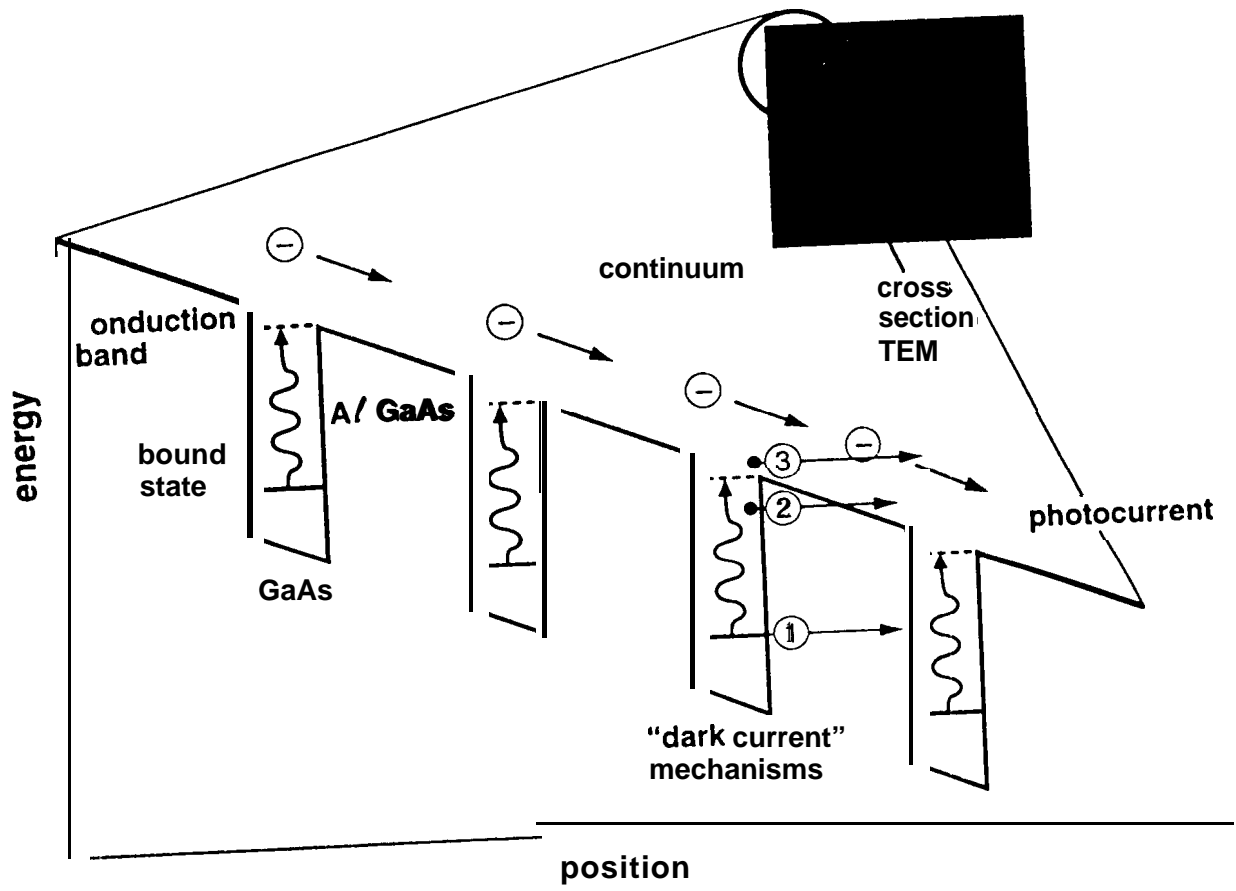


Fig 1

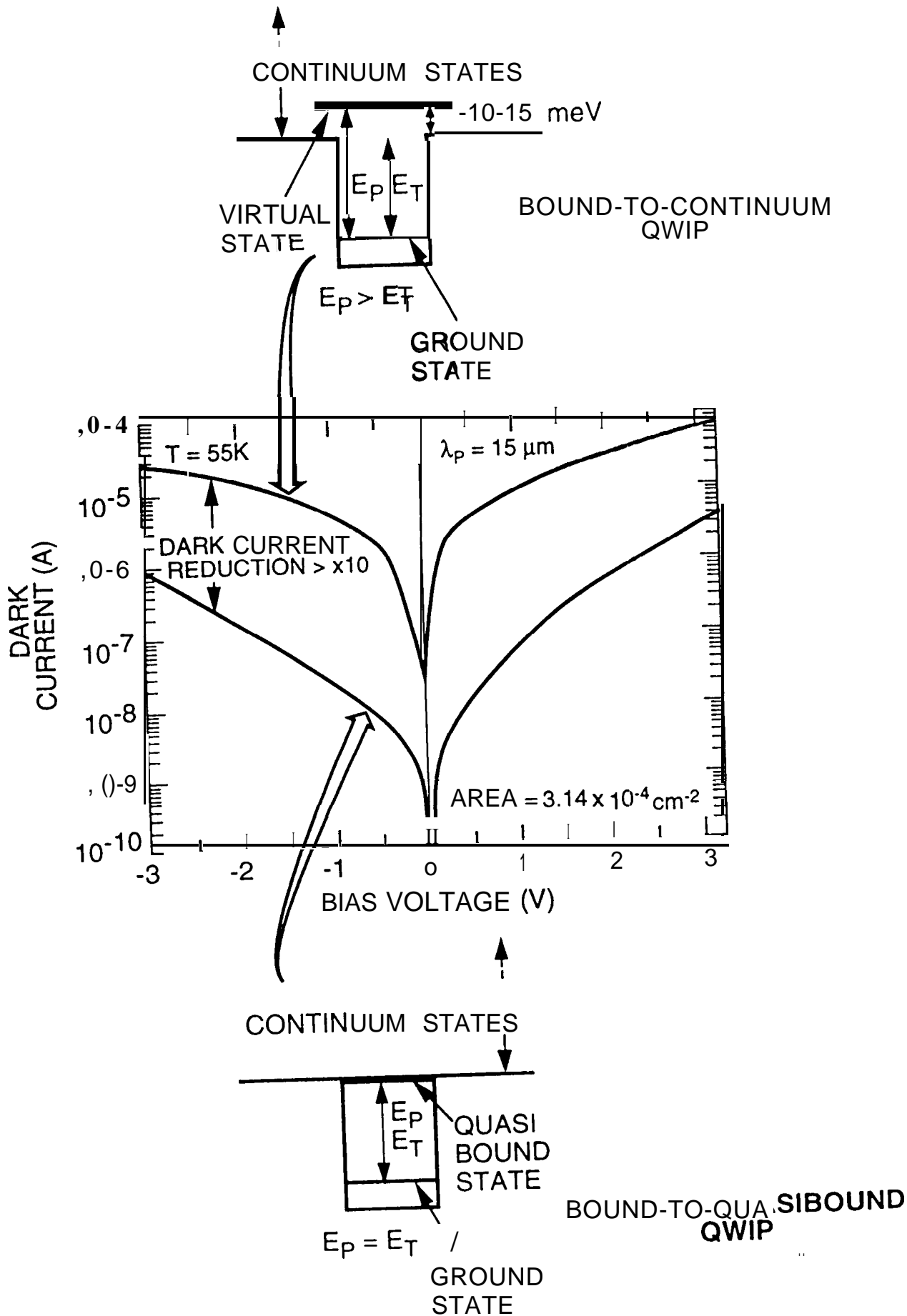


Fig 2

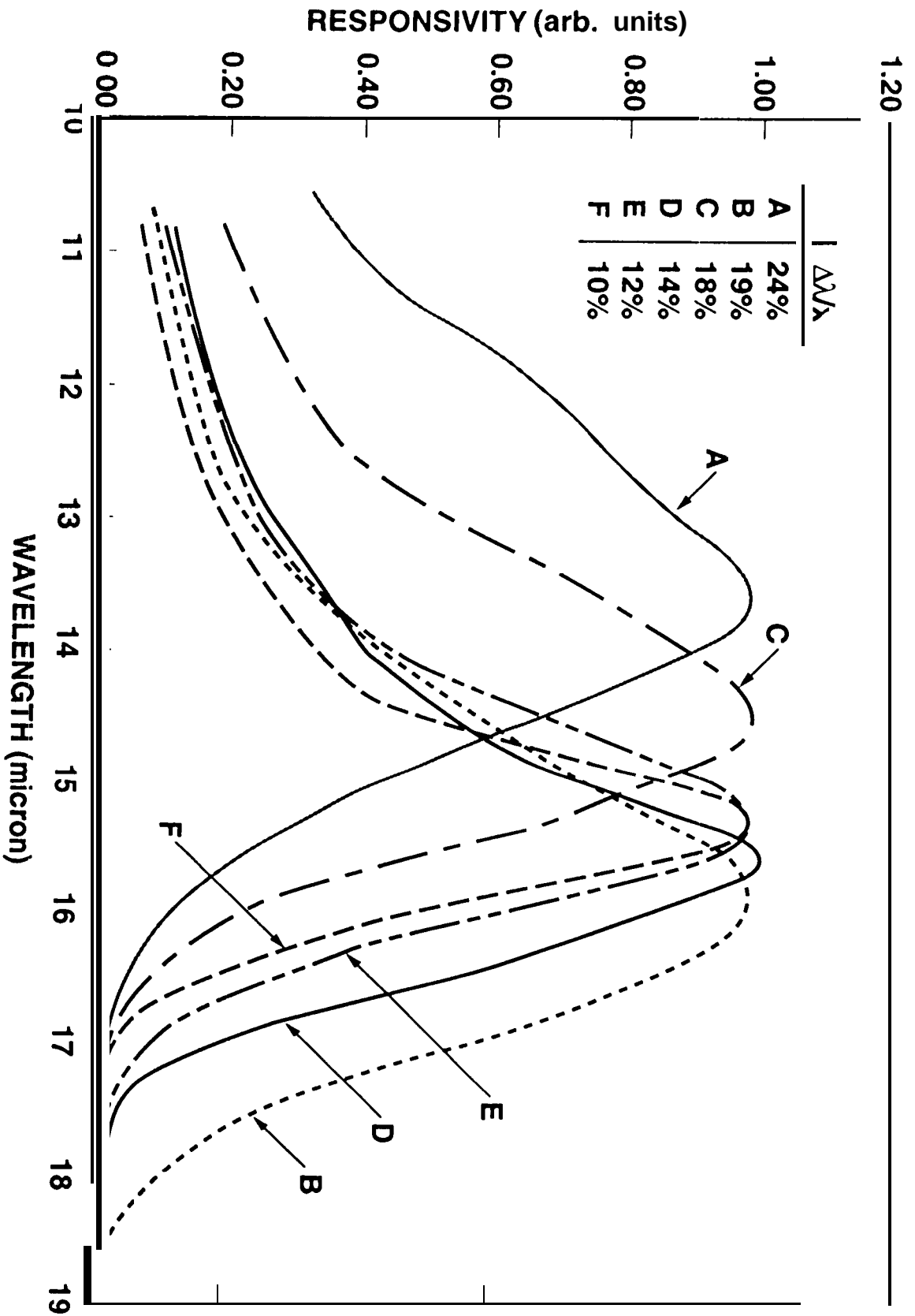
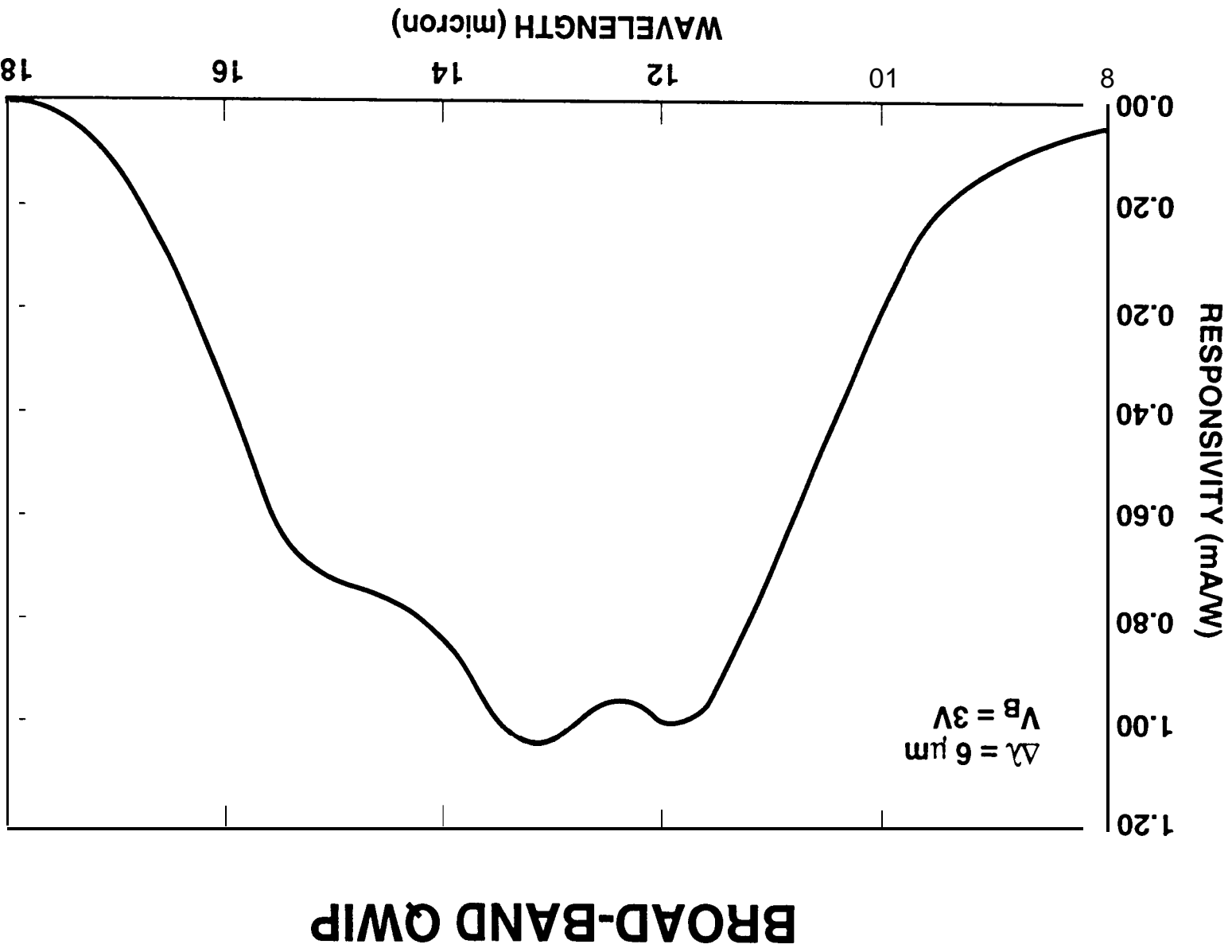


Fig 3

Fig 4



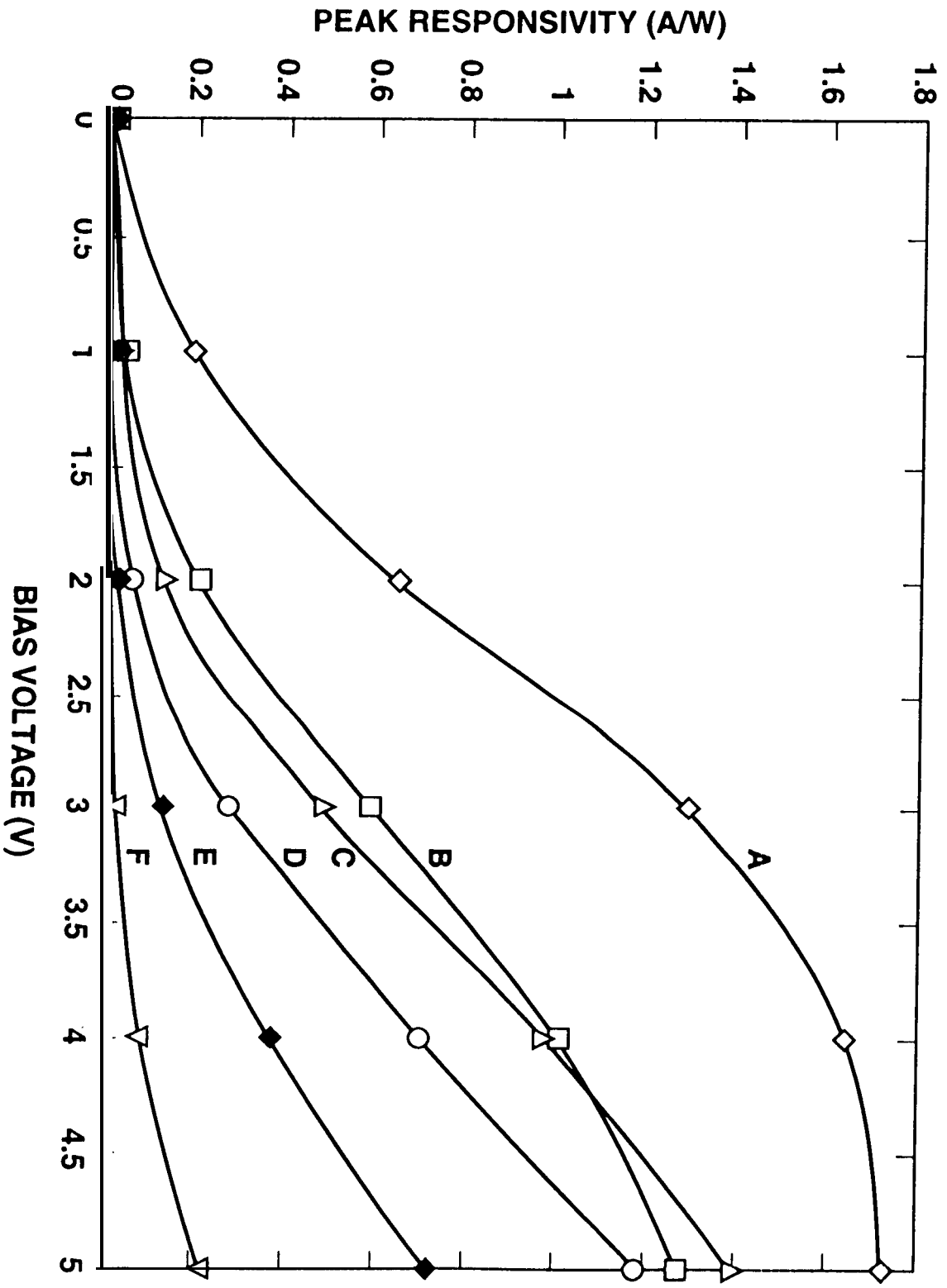


Fig 5

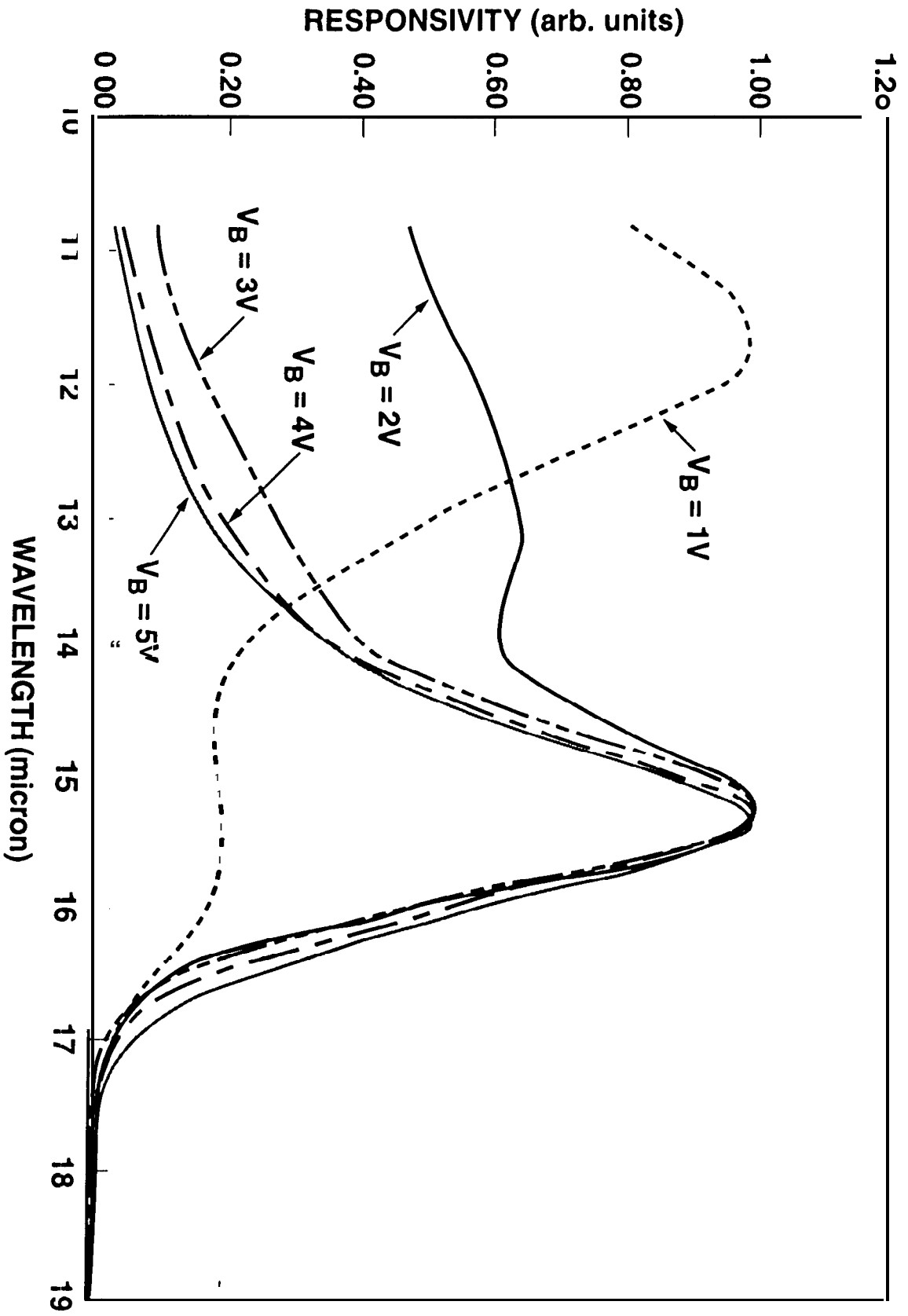
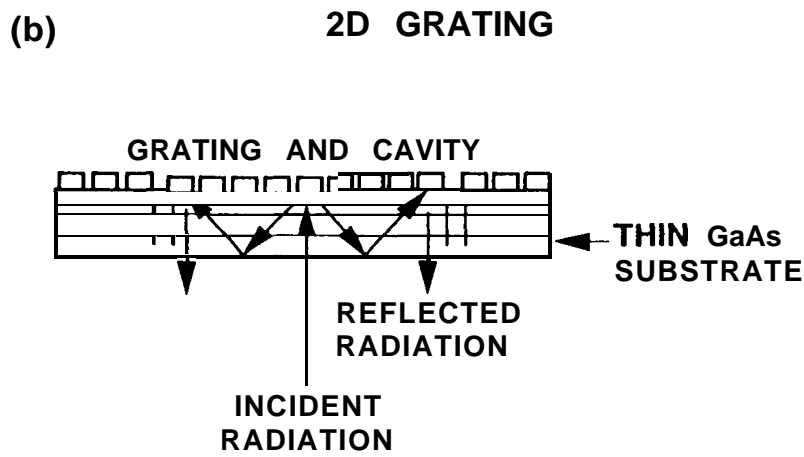
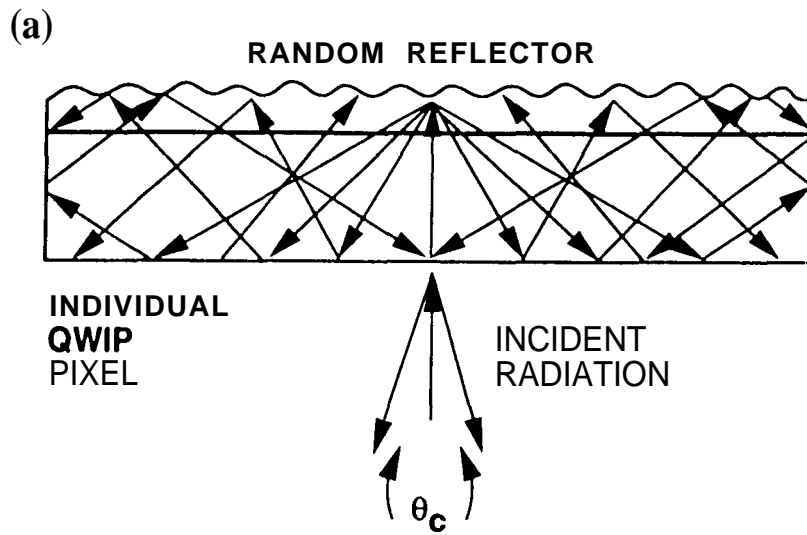


Fig 6



BD-07

Fig 7

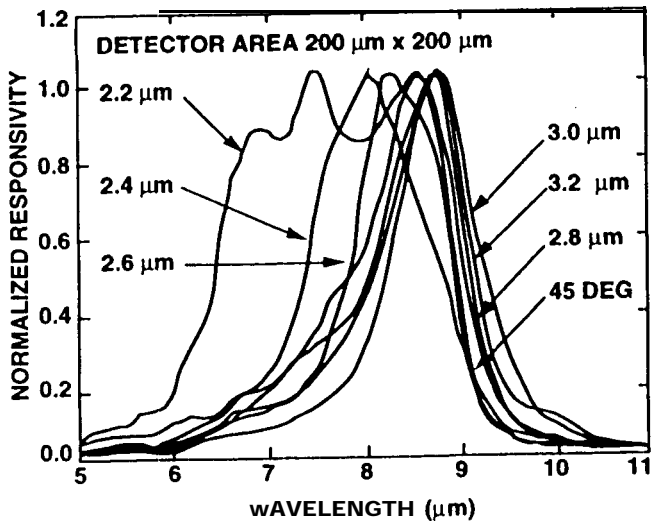


Fig 8

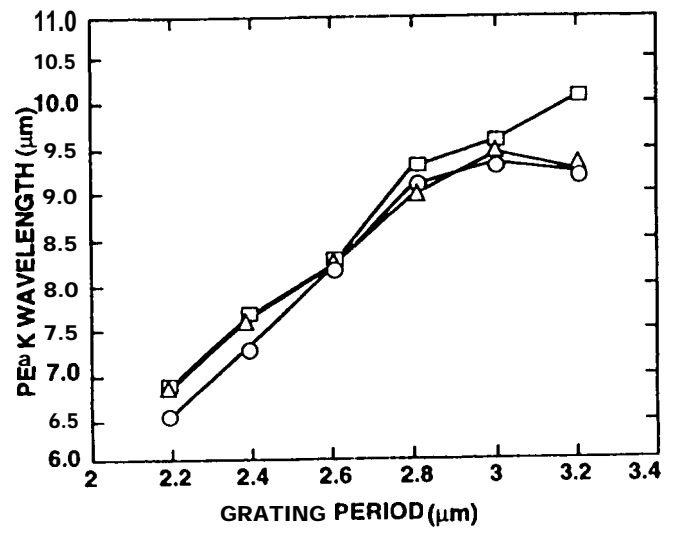


Fig 9

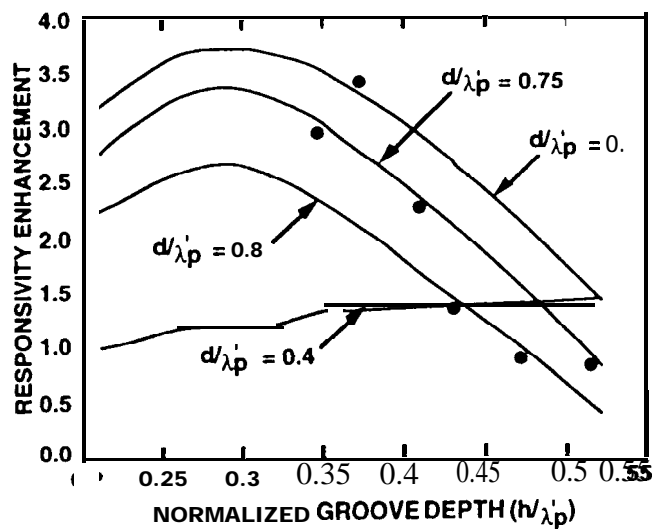


Fig 10